



This is a repository copy of *Structure of NaFeSiO₄, NaFeSi₂O₆, and NaFeSi₃O₈ glasses and glass-ceramics.*

White Rose Research Online URL for this paper:
<https://eprints.whiterose.ac.uk/165755/>

Version: Accepted Version

Article:

Ahmadzadeh, M., Scrimshire, A., Mottram, L. et al. (4 more authors) (2020) Structure of NaFeSiO₄, NaFeSi₂O₆, and NaFeSi₃O₈ glasses and glass-ceramics. *American Mineralogist*, 105 (9). pp. 1375-1384. ISSN 0003-004X

<https://doi.org/10.2138/am-2020-7285>

© 2020 Mineralogical Society of America. This is an author-produced version of a paper subsequently published in *American Mineralogist*. Uploaded in accordance with the publisher's self-archiving policy.

Reuse

Items deposited in White Rose Research Online are protected by copyright, with all rights reserved unless indicated otherwise. They may be downloaded and/or printed for private study, or other acts as permitted by national copyright laws. The publisher or other rights holders may allow further reproduction and re-use of the full text version. This is indicated by the licence information on the White Rose Research Online record for the item.

Takedown

If you consider content in White Rose Research Online to be in breach of UK law, please notify us by emailing eprints@whiterose.ac.uk including the URL of the record and the reason for the withdrawal request.



eprints@whiterose.ac.uk
<https://eprints.whiterose.ac.uk/>

Structure of NaFeSiO₄, NaFeSi₂O₆, and NaFeSi₃O₈ glasses and glass-ceramics

(American Mineralogist, Accepted Manuscript, 2020)

**Mostafa Ahmadzadeh,^{a,c} Alex Scrimshire,^b Lucy Mottram,^d Martin C. Stennett,^d Neil C.
Hyatt,^d Paul A. Bingham,^b John S. McCloy^{a,c,d,e,*}**

^aMaterials Science and Engineering Program, Washington State University, Pullman, WA, 99164, USA

^bMaterials and Engineering Research Institute, Sheffield Hallam University, Sheffield S1 1WB, UK

^cSchool of Mechanical and Materials Engineering, Washington State University, Pullman, WA, 99164,
USA

^dDepartment of Materials Science and Engineering, The University of Sheffield, Sheffield, S1 3JD, UK

^eInstitut de Physique du Globe de Paris, Équipe Géomatériaux, Paris, France

* Corresponding author, E-mail address: john.mccloy@wsu.edu

ABSTRACT

The crystallization of iron-containing sodium silicate phases holds particular importance, both in the management high-level nuclear wastes and in geosciences. Here, we study three as-quenched glasses and their heat-treated chemical analogues, NaFeSiO_4 , $\text{NaFeSi}_2\text{O}_6$, and $\text{NaFeSi}_3\text{O}_8$ (with nominal stoichiometries from feldspathoid, pyroxene, and feldspar mineral groups – i.e., $\text{Si/Fe} = 1, 2,$ and 3 respectively) – using a variety of techniques. Phase analyses revealed that as-quenched NaFeSiO_4 cannot accommodate all Fe in the glass phase (some Fe crystallizes as Fe_3O_4), whereas as-quenched $\text{NaFeSi}_2\text{O}_6$ and $\text{NaFeSi}_3\text{O}_8$ form amorphous glasses upon quenching. $\text{NaFeSi}_2\text{O}_6$ glass is the only composition that crystallizes into its respective isochemical crystalline polymorph, i.e. aegirine, upon isothermal heat-treatment. As revealed by Mössbauer spectroscopy, iron is predominantly present as 4-coordinated Fe^{3+} in all glasses, though it is present as 6-coordinated Fe^{3+} in the aegirine crystals ($\text{NaFeSi}_2\text{O}_6$), as expected from crystallography. Thus, Fe can form the crystalline phases in which it is octahedrally coordinated, even though it is mostly tetrahedrally coordinated in the parent glasses. Thermal behavior, magnetic properties, iron redox state (including Fe K-edge X-ray absorption), and vibrational properties (Raman spectra) of the above compositions are discussed.

Keywords: Mössbauer, Fe redox, Raman, glass transition

INTRODUCTION

Crystallization of iron-containing sodium silicate phases is important, both in the management of high-level nuclear wastes and in geosciences (Ahmadzadeh et al., 2017; Bailey and Schairer, 1963; Bailey and Schairer, 1966; Cochain et al., 2012; Jantzen, 2011; Jantzen and Brown, 2007; Jeoung et al., 2001). The complex high-level nuclear wastes (HLW) stored in steel tanks at the Hanford site can contain more than 20 elements, among which iron (Fe) concentrations vary from about 5 to more than 30 wt% Fe_2O_3 , for high-Al and high-Fe HLW, respectively (Kim et al., 2011; Kruger et al., 2013). Within the high-Fe wastes, Na_2O concentration varies from about 10 to 20 wt% depending on the cluster (Kim et al., 2011). Vitrification is the process used to immobilize radioactive HLW by converting it into a solid stable glass. SiO_2 is added in considerable amounts (with lower levels of other additives) to vitrify the radioactive HLW into a glass for immobilization. Consequently, HLW glasses have high concentrations of Si, Fe, and Na, and are thus potentially prone to crystallization of iron sodium silicate phases.

In particular, aegirine ($\text{NaFeSi}_2\text{O}_6$, also known as acmite), which is a clinopyroxene silicate phase, has been known to crystallize within some HLW glasses (Hrma et al., 1999; Jantzen and Edwards, 2015; Jantzen and Bickford, 1984; Jantzen et al., 1984; Vienna et al., 1996). Studying the crystallization of more than 100 simulants HLW glass compositions, Kim et al. (1994) reported that aegirine forms upon isothermal heat-treatment of glasses with high Na_2O (>10 wt%) and Fe_2O_3 (>7 wt%) contents, while aegirine is not observed in samples that have been canister-centerline-cooled (slow cooling profile recorded at the centerline of the Hanford HLW canisters). Surface crystallization of aegirine from simplified HLW glasses was confirmed by Plaisted et al. (2000), who showed that the aegirine contains other elements such as Cr and Ni and that its composition varies by temperature of the heat treatment. The formation of aegirine causes a small

to moderate decrease in the chemical durability of final HLW glass waste form (Jantzen and Bickford, 1984; Jantzen et al., 1984; Jantzen et al., 2010). The spinel formation (i.e., magnetite Fe_3O_4 and related phases), however, has little or no effect on glass durability, whereas nepheline (NaAlSiO_4) and related aluminosilicate phases have the most detrimental impacts on aqueous chemical durability of crystallized HLW glass.

Iron and sodium are among the most common constituents of natural silicate melts, and both can have remarkable effects on their physical properties. Bailey and Schairer (1966) have extensively described how equilibrium crystalline and liquid phases in the system $\text{Na}_2\text{O}-\text{Al}_2\text{O}_3-\text{Fe}_2\text{O}_3-\text{SiO}_2$ are petrologically important for a wide range of alkaline igneous rocks. These crystalline phases include aegirine ($\text{NaFeSi}_2\text{O}_6$), 5.1.8 ($5\text{Na}_2\text{O}\cdot\text{Fe}_2\text{O}_3\cdot 8\text{SiO}_2$ or $\text{Na}_5\text{FeSi}_4\text{O}_{12}$), nepheline (NaAlSiO_4 , hexagonal), carnegieite (NaAlSiO_4 , orthorhombic), albite ($\text{NaAlSi}_3\text{O}_8$), sodium metasilicate (Na_2SiO_3), hematite (Fe_2O_3), and different polymorphs of SiO_2 (quartz, tridymite, and cristobalite). In such a system, Fe^{3+} can potentially behave similarly to Al^{3+} , though iron can play a special role; each valence state of iron plays a different structural role, and the redox ratio ($\text{Fe}^{3+}/\text{Fe}^{2+}$), can consequently influence the melting and crystallization behavior of magmas and properties of igneous rocks (Mysen and Richet, 2005). Hence, studying the speciation and structural role of Fe is crucial in understanding the structure of iron-containing silicate melts and glasses and their crystallization behavior (Komatsu and Soga, 1980).

Aegirine, a chain silicate from the clinopyroxene group, is the most well-studied sodium iron silicate phase. It melts incongruently, with separation of hematite at 990°C (Bowen et al., 1930) and has a monoclinic symmetry with space group $C2/c$ (Clark et al., 1969). Aegirine is the mineral name for the Na- Fe^{3+} end-member of the class of rock-forming pyroxene minerals which in nature typically contains some impurities of Al, Cr, and Ca. The mineral aegirine is less common

than other mixed metal Ca-Mg-Fe pyroxenes, such as augite, but is an important minor component (Bailey and Schairer, 1966; Bowen et al., 1930; Deer et al., 1992; Larsen, 1976). Another sodium iron silicate phase, known as 5.1.8 ($\text{Na}_5\text{FeSi}_4\text{O}_{12}$), has not been reported to occur in natural rocks. The “5.1.8” composition was first discovered by Bowen et al. (1930), and is extensively studied in our previous work (Ahmadzadeh et al., 2018).

In the sodium alumino-silicate groups, there are three important types of well-known minerals based on their SiO_2 content; nepheline or carnegieite (NaAlSiO_4 , feldspathoid), jadeite ($\text{NaAlSi}_2\text{O}_6$, pyroxene), and albite ($\text{NaAlSi}_3\text{O}_8$, feldspar). Aegirine is the iron “equivalent” of jadeite, with the same crystal structure in which Fe^{3+} substitutes for Al^{3+} depending upon the pressure, though end-member jadeite is difficult to form except under extreme conditions (Nestola et al., 2007). NaFeSiO_4 (Fe-nepheline) and $\text{NaFeSi}_3\text{O}_8$ (Fe-albite) do not exist as known crystalline phases.

The present work describes crystallization studies of the three feldspathoid-, pyroxene-, and feldspar-type sodium iron silicate compositions. The structure of the parent glasses and the corresponding phases which form upon heat-treating the glasses are discussed. It should be noted that controlling the melting and/or heat-treatment atmosphere, and the subsequent Fe oxidation state, was not the aim of this work. The crystallization behavior of these compounds and the role of iron are presented through thermal analysis, X-ray diffraction, Raman, Mössbauer and X-ray absorption spectroscopies, and magnetic property measurements.

MATERIALS AND METHODS

Glasses nominally isochemical with the compositions of NaFeSiO_4 (‘Fe-nepheline’), $\text{NaFeSi}_2\text{O}_6$ (aegirine), and $\text{NaFeSi}_3\text{O}_8$ (‘Fe-albite’) were synthesized from Na_2CO_3 (Fisher Scientific, >99%), Fe_2O_3 (Alfa Aesar, 98%), and SiO_2 (U.S. Silica, 99.7%) powders as starting

materials. Each batch was melted twice for one hour in air in an electric furnace at 1500°C in platinum-10% rhodium crucibles, to make ~ 20 g of glass. Each melt was poured onto an Inconel plate to quench and form a glass. In the case of the Fe-nepheline composition, the melt was quenched more rapidly between two brass plates in order to attempt to avoid formation of Fe₃O₄ (magnetite), which was not completely achievable. The quenched glasses were then crushed into powders and isothermally heat-treated in the specific conditions selected to attempt to obtain maximum crystallization. The Fe-nepheline glass was heat-treated at 775°C for 7 h based on our previous study (Ahmadzadeh et al., 2017). The aegirine glass was heat treated at 900°C for 24 h based on the available phase diagrams in the literature (Bowen et al., 1930). The Fe-albite glass was heat treated at 1000°C for 24 h due to its higher SiO₂ content and known difficulty for nucleating its Al analogue, albite. In another test, this glass was also kept in the furnace for a longer time (72 h) at 900°C in an attempt to form the isochemical crystalline polymorph. All heat-treatments were followed by quenching samples in air. The compositions, melting temperatures, and heat-treatment conditions are summarized in Table 1.

For differential thermal analysis (DTA) and thermogravimetric analysis (TGA), the as-quenched glasses were crushed and sieved to a particle range of 63 to 125 µm. The data were obtained with a heating rate of 10°C min⁻¹ under constant N₂ flow (99.998% pure) with a SDT Q600–TA Instruments system.

An X'Pert Pro MPD (PANalytical, Netherlands) was employed to collect powder X-ray diffraction (XRD) patterns with Co K α X-rays ($\lambda = 0.1789$ nm) at 40 kV and 40 mA, and data were analyzed using HighScore Plus software (PANalytical, Netherlands). For semi-quantitative Rietveld refinement and quantification of the phase fractions, powders were mixed with 10 wt % CaF₂ as an internal standard.

Magnetic hysteresis loops were obtained using a vibrating sample magnetometer (VSM, PMC3900, Lakeshore Cryotronics, Westerville, OH) with maximum applied field of 1.8 T.

Room temperature ^{57}Fe Mössbauer spectra were collected relative to $\alpha\text{-Fe}$ over a velocity range of ± 12 or ± 6 mm s^{-1} using a constant acceleration spectrometer with a 25 mCi source of ^{57}Co in Rh. Attempts were made to fit the spectra using Lorentzian as well as Extended Voigt-Based Fitting (xVBF) paramagnetic doublets consistent with Fe^{3+} and/or Fe^{2+} , using the Recoil analysis software package (Rancourt, 1998). The area ratio of the doublets was established, enabling estimation of the $(\text{Fe}^{3+}/\Sigma\text{Fe})$ redox ratio based on fitted peak areas and assuming that the recoil-free fraction ratio $f(\text{Fe}^{3+})/f(\text{Fe}^{2+}) = 1.0$.

For iron redox ratio analysis, in addition to Mössbauer spectroscopy, a solution-based spectrophotometric method (wet chemistry) was used. The reported average and standard deviation values are obtained from three replicate measurements of each sample. The procedure details are given in (Ahmadzadeh et al., 2018; Weaver et al., 2015) and references therein.

Fe K-edge X-ray absorption near edge structure (XANES) data were collected on the Beamline for Materials Measurement (bending magnet beamline BM-6) at the National Synchrotron Light Source II (NSLS II), Brookhaven National Laboratory, Upton, New York State, USA. The beamline is configured with a Rh-coated paraboloid collimating mirror, a Si (111) monochromator, and a flat harmonic rejection mirror. XANES data were acquired in transmission mode; an array of three ionization chambers, filled with N_2 and operated in a stable region of their current vs voltage curve, enabled concurrent measurement of incident and transmitted beam intensities from both a sample and a reference Fe foil. Measurements were made in air at room temperature with the sample orientated at an incidence angle of 45° to the beam. Samples were prepared from finely ground powder specimens. These were homogeneously dispersed in 60 mg of

polyethylene glycol (PEG) and pressed in a 13 mm diameter die, to produce a thickness of one absorption length. Further details on data treatment of the XAS data, including the pre-edge, is described in the supplementary.

Raman spectra were collected on a Jobin Yvon-SPEX Horiba T64000 triple-spectrometer with confocal system through an Olympus BX40 microscope. Samples were excited using a 488 nm Coherent Genesis MX SLM laser running at 500 mW output power. The detector was a liquid nitrogen cooled CCD camera. The spectrometer was calibrated using the 520 cm^{-1} line of single crystal silicon to within 1 cm^{-1} . Spectra were collected through a 200 x objective lens, from 25-1300 cm^{-1} , for count times of 200 s, with three subsequent spectra averaged.

RESULTS

Phase Analysis

X-ray diffraction patterns were obtained for the as-quenched (AQ) and heat-treated (HT) samples (See supplementary, Figure S1). Table 2 summarizes phase analysis of the three compositions, based on their XRD and Rietveld refinement results. As described in Table 2, depending on the ratio of Si to Fe, the as-quenched samples make either an amorphous phase (for Fe-albite and aegirine) or precipitate some iron as magnetite (for Fe-nepheline). Upon heat-treating the as-quenched samples, they may form hematite and/or aegirine, depending on the composition.

Thermal Analysis

The DTA and TGA results of the three as-quenched glasses are presented in supplementary, Figure S2. Increasing the SiO_2 content leads to an increase in the glass transition temperature, T_g , of the amorphous phases, which is characterized by a subtle endothermic drop in the DTA thermographs, from 471°C in NaFeSiO_4 , to 498°C in $\text{NaFeSi}_2\text{O}_6$, to 521°C in $\text{NaFeSi}_3\text{O}_8$

glasses. The T_g decrease is probably related to overall decrease in average bond strength, since Fe-O bonds (both with Fe^{2+} and Fe^{3+}) are considerably weaker than Si-O bonds (Luo and Kerr, 2006). Other observations about the thermal behavior are given in the supplementary.

Magnetic Measurements

Magnetization as a function of magnetic field measurements at room temperature (Figure 1) reveal that Fe-albite and aegirine as-quenched glasses contain no iron oxide (paramagnetic), whereas the as-quenched Fe-nepheline contains considerable amount of magnetite (ferrimagnetic). Further observations are provided in the supplementary.

Mössbauer Spectroscopy

Room temperature Mössbauer spectra of Fe-nepheline, aegirine, and Fe-albite as-quenched samples and crystallized aegirine sample were obtained (Figure 2). The fitted Mössbauer spectral parameters are given in the supplementary (Table S1). Aegirine and Fe-albite glasses and crystallized aegirine were fitted by two overlapping doublets, whereas the as-quenched Fe-nepheline was fitted by one doublet plus two sextets characteristic of magnetite (Fe_3O_4) (Oh et al., 1998). As-quenched aegirine and Fe-albite samples (Figure 2b and c) were fitted by xVBF functions, because at least three doublets were required in order to obtain robust fits using Lorentzian lines, and xVBF has also been successfully used to fit Mössbauer spectra for similar materials (Forder et al., 2013). This method provided robust fits with acceptable χ^2 using only two doublets to fit the glass spectrum, one each representing Fe^{2+} (lower intensity) and Fe^{3+} (higher intensity), according to their chemical shift (CS) and quadrupole splitting (QS) values obtained from the fits (Dyar, 1985; Dyar et al., 2006; Mysen and Richet, 2005).

Such ^{57}Fe Mössbauer behavior, shown in Figure 2, is typical for iron-containing silicate glasses (Mysen and Richet, 2005). The fitted CS and QS values also reveal that the Fe^{3+} and Fe^{2+}

are predominantly tetrahedrally coordinated in these glasses, though Fe^{2+} can possibly have some five-fold coordination. In the spectrum for the Fe-nepheline as-quenched sample, there is an intense doublet assigned to four-coordinated Fe^{3+} in the glass phase, in addition to the sextets attributed to the magnetite phase.

The crystallized aegirine sample shown in Figure 2d (fitted using Lorentzian peaks) exhibits a new strong doublet, in addition to the primary four-coordinated Fe^{3+} doublet which is also observed in the glass sample. The new doublet, showing significantly lower QS and higher CS (0.40 and 0.31 mm/s, respectively), is due to octahedrally-coordinated Fe^{3+} from crystalline aegirine, as Fe^{3+} arranges 6-coordinated in this phase (Cameron et al., 1973). Considering the experimental error, these values are consistent with the QS and CS values reported in the literature (e.g., in (Baum et al., 1988), 0.39 and 0.33 mm/s, respectively) for pure aegirine crystals at room temperature. Overall, in the studied sodium iron silicate glasses, iron is shown to be predominantly present as four-fold coordinated Fe^{3+} ($^4\text{Fe}^{3+}$), whereas crystal chemistry dictates the iron redox state and coordination in the crystalline phase(s). Table S2 (see supplementary) presents the measured iron redox values of the two crystal-free samples, i.e., aegirine and Fe-albite glasses, obtained from the wet chemistry method, compared to those estimated from Mössbauer spectroscopy. Note that the iron redox values from Mössbauer spectroscopy are derived from the xVBF fits. The redox states from both methods are consistent, and aegirine glass shows slightly higher $\text{Fe}^{3+}/\Sigma\text{Fe}$ ratio than Fe-albite glass.

X-ray Absorption

Figure 3 shows the results of the Fe K-edge data and analysis, including the XANES spectra (a), the extracted pre-edge features (b), and the structure field diagram of pre-edge centroid energy position and integrated intensity (c). The latter diagram gives an indication of Fe redox state and

coordination number (CN). Qualitative comparison with the standard spectra for Fe^{3+} , CN=6 ($^{61}\text{Fe}^{3+}$, aegirine, natural mineral, $\text{NaFeSi}_2\text{O}_6$), Fe^{3+} , CN=4 ($^{41}\text{Fe}^{3+}$, FePO_4 , synthetic), Fe^{2+} , CN=6 ($^{61}\text{Fe}^{2+}$, FeCO_3 , synthetic), and Fe^{2+} , CN=4 ($^{41}\text{Fe}^{2+}$, staurolite, natural mineral, $\text{Fe}_{1.5}\text{Mg}_{0.5}\text{Al}_9\text{Si}_{3.9}\text{Al}_{0.1}\text{O}_{22}(\text{OH})_2$), indicates that the iron in the glasses mostly exists as $^{41}\text{Fe}^{3+}$. In general, the determined centroid energy and integrated intensity of the weak pre-edge features measured from our reference crystalline compounds are in good agreement with those reported by (Wilke et al., 2001), with the exception of our FePO_4 standard for which we determine a greater integrated intensity, most likely due to an overly thick sample resulting in a relatively suppressed edge step.

The weak pre-edge feature is associated with electronic transitions occurring between the 1s and 3d energy levels, and is a feature common to the K-edge spectra of many transition metals (Yamamoto, 2008). Lower oxidation states have fewer unfilled 3d levels, so transitions from the 1s levels become less probable and the intensity of this feature becomes less well-defined; these transitions are only weakly allowed for octahedral Fe since the initial and final states are centrosymmetric; whereas, for Fe in a non-centrosymmetric tetrahedral environment, the transition probability is enhanced due to admixture of unoccupied 4p orbitals in the final state. Previously, careful measurements of crystalline standards have been made (Wilke et al., 2001), showing the relationship between Fe valence and coordination and pre-edge position and intensity, and further applied to glasses (Farges et al., 2004). It has also been shown that the extraction of Fe redox and coordination number from Fe XAS pre-edge features is complicated by monochromator resolution limitations (Cottrell et al., 2009; Galois et al., 2001; Wilke et al., 2005) and fitting method. Recent inter-synchrotron comparison of a set of reference glasses shows that with careful measurements and fitting procedures, an uncertainty in the centroid of ± 0.1 eV is achievable (Fiege et al., 2017).

Raman Spectroscopy

The raw Raman spectra of the as-quenched glasses are shown in Figure 4. All of these spectra show a background decreasing in intensity from low to high Raman shifts. Di Muro et al. (2009) have studied a number of Fe-containing natural glasses and shown that the background slope of the raw Raman spectra correlates with the total iron content and its redox within the glasses. Figure 4 reveals a consistent trend for our samples; the slope of the background increases with increasing the Fe content and its redox state ($\text{Fe}^{3+}/\Sigma\text{Fe}$) from Fe-albite to Fe-nepheline.

The Raman spectra of the three as-quenched glasses (Figure 4) show intense low frequency envelopes with at least two bands; a main peak at $\sim 440\text{-}460\text{ cm}^{-1}$ and a shoulder at $530\text{-}550\text{ cm}^{-1}$. The main peak at $\sim 450\text{ cm}^{-1}$, which was shown to be a polarized band by (Wang et al., 1993) for similar compositions, is assigned to the vibrations of bridging oxygens (BOs), i.e. (T–O–T), where T=Si,Fe, in tetrahedral rings. The high frequency (HF) band of the three spectra consists of a dominant peak at $900\text{-}960\text{ cm}^{-1}$ and a shoulder at higher frequencies, i.e., $\sim 1040\text{-}1100\text{ cm}^{-1}$. Wang et al. (1993; 1995), have shown for similar compositions that the dominant peak is depolarized whereas the shoulder is polarized, suggesting that the dominant peak is for the antisymmetric T–O–T stretching vibrations of BOs ($\nu_{\text{as}}(\text{T–O–T})$), and the shoulder originates from the symmetric stretching vibrations of NBOs. This is a similar conclusion to that reached earlier by Mysen et al. (1980), who measured an aegirine glass spectrum similar to that shown here, with slightly greater intensity of the higher frequency band, though these authors attributed both bands to stretching of BOs, with one in a Fe-rich and the other in a Si-rich environment.

It can also be seen in Figure 4 that increasing SiO_2 content systematically increases the frequency of HF envelope. This shift is related to decreased number of heavier Fe^{3+} tetrahedra (as opposed to lighter Si^{4+} tetrahedra) in the Fe-albite sample which lead to increased vibration

frequencies (i.e., Raman shift). The HF envelope contains not only the silicate tetrahedral bands, Q^n , where n is the number of bridging oxygens, but also the $^{[4]}Fe^{3+}$ related band, generally thought to be $\sim 910-980\text{ cm}^{-1}$ (Baert et al., 2011; Cochain et al., 2008; Di Genova et al., 2017; Magnien et al., 2006), near the lower frequency end of the band and hence weighting the envelope to lower frequencies when the tetrahedral Fe^{3+} concentration is high. This band attributed to $^{[4]}Fe^{3+}$ has been reported to shift to lower frequencies as Fe concentration is increased (Cochain et al., 2008), and does here as well (peak of Raman spectrum moves 965 cm^{-1} , 950 cm^{-1} , 920 cm^{-1} , for Fe-albite, aegirine, Fe-nepheline glasses, respectively), though there is some contribution of the silicate stretches. A Raman band attributed to Fe^{2+} contributions has been reported at $1040-1050\text{ cm}^{-1}$ (Cochain et al., 2008; Di Genova et al., 2017); however, the significant Raman scattering observed in this region in the Fe-nepheline glass is due rather to the Si-O stretching, since the peak of the Raman spectrum for a $NaAlSiO_4$ glass lies $\sim 1015\text{ cm}^{-1}$ when measured on the same instrument (not shown).

DISCUSSION

As-quenched glasses

As confirmed by XRD and magnetic measurements, $NaFeSi_2O_6$ and $NaFeSi_3O_8$ compositions have sufficient Si content to make pure glasses during quenching, while molten $NaFeSiO_4$ cannot readily quench into a glass at our quenching rate, without crystallization of excessive Fe as magnetite. Mössbauer spectroscopy revealed that iron in these glasses is predominantly present as tetrahedrally coordinated Fe^{3+} , while some Fe^{2+} with higher coordination may also exist. Preparation of silicate glasses in which 100% of the iron is present as Fe^{3+} can only be accessed under normal laboratory melting conditions if oxidizing agents (for example CeO_2) are added to the batch (Bingham et al., 2014), or if glasses with high basicity (i.e., high alkali

contents) are used. Similar Mössbauer results to ours are reported by Fleet et al. (1984) and Henderson et al. (1984) for Fe-albite glass melted at 1450°C and 1 bar, though they used Lorentzian functions to fit their data, possibly resulting in lower reduced iron (~9% Fe²⁺) than our measurements (~19% Fe²⁺). Using neutron diffraction experiments and Empirical Potential Structure Refinement (EPSR) modeling, Weigel et al. (Weigel et al., 2008b; Weigel et al., 2006) have discussed that, in their aegirine glass melted at 1450°C for 30 min in air, the majority of Fe³⁺ (~95%) is four-coordinated with oxygen, some Fe³⁺ (~5%) is five-coordinated, and all Fe²⁺ is five-coordinated. Their results also showed that ^{[4]Fe³⁺} is randomly distributed in the glass network, acting as a network former. These temperatures are sufficiently close to our melting temperature (1500°C) that redox ratios obtained upon quenching should be similar (~12% Fe²⁺ (Weigel et al., 2008a) vs. ~15% Fe²⁺ our measurements), if redox equilibrium with the surrounding atmosphere was obtained or approached in both cases.

The XAS pre-edge results of our as-quenched glasses shown in Figure 3 indicate that, while iron primarily exists as Fe³⁺ based on the centroid positions of the glasses, the centroids are slightly shifted towards Fe²⁺ (lower energies) compared to the reference compounds. This is consistent with the presence of some Fe²⁺ obtained from Mössbauer and wet chemistry colorimetric data, and consistent with the ‘mixing curves’ for ^{[4]Fe³⁺} and ^{[4]Fe²⁺} in silicate glasses (Jackson et al., 2005). However, no difference in the position of the centroids of the three studied glasses can be ascertained. This implies that the small differences between redox of these three materials are not distinguishable from the pre-edge results at this spectrometer resolution. Indeed, the shift from the Fe redox glass standards recently reported (Fiege et al., 2017) suggests that at most a 0.2 eV shift would be expected for glasses with Fe³⁺/∑Fe of 80 to 100%. Moreover, the integrated intensities of the glasses, as shown in Figure 3-c, do not vary sufficiently to be able to make a meaningful

interpretation of change, if any, of Fe coordination numbers. Our XAS data therefore demonstrate the speciation of Fe in the glasses to be predominantly $^{[4]}\text{Fe}^{3+}$ with some Fe^{2+} , probably $^{[4]}\text{Fe}^{2+}$, contribution. It should be noted, however, that some have suggested that Fe coordination in silicate glasses is between 4 and 5 for both Fe^{3+} and Fe^{2+} (Bychkov et al., 1993; Farges et al., 2005; Liu and Lange, 2006).

Fe redox ratio in melts is a function of temperature, pressure, composition, and oxygen fugacity (Mysen and Richet, 2005). We calculated the Fe redox ratio of the present glasses based on the equation provided by Jayasuriya et al. (2004), assuming the oxygen fugacity of $10^{-0.7}$ for air. The $\text{Fe}^{3+}/\Sigma\text{Fe}$ values predicted are 66.3% (Fe-albite), 72.5% (aegirine), compared to measured values of 81.5% (Fe-albite, wet chemistry) and 83.3% (aegirine glass, wet chemistry) (Table S2). Other classic equations such as that of Sack et al. (1980) was also used, but the Fe^{2+} computed is larger than those of Jayasuriya equation (Jayasuriya et al., 2004), and the latter is closer to the measured values for the current compositions.

Our Fe-nepheline as-quenched sample only shows Fe^{3+} in the glass according to the Mössbauer results, unlike the other two compositions, while the calculations for this composition show $\text{Fe}^{3+}/\Sigma\text{Fe}$ of 81.9% for the melt at 1500°C. In the Fe-nepheline melt, the present Fe^{2+} in the melt partitioned into magnetite ($\text{Fe}^{2+}\text{O} \cdot \text{Fe}_2^{3+}\text{O}_3$) while it was being quenched, and only Fe^{3+} remained in the glass phase. If partial crystallization takes place during quench, the redox ratio of the glass is different from that of its parent melt (Mysen and Richet, 2005).

Increasing $\text{Fe}^{3+}/\Sigma\text{Fe}$ with increasing iron content observed in these iron-bearing silicate glasses is partially due to the following. Having less SiO_2 as the main glass former encourages the iron (which is now at a larger fraction) to take a network forming role, and thus Fe^{3+} . Systematic decrease in the vibrational frequency of the HF Raman band by decreasing the Si/Fe ratio confirms

increased number of heavier Fe^{3+} network formers (i.e., tetrahedra). The same Raman trend has been reported by Wang et al. (1993) for similar compositions. They have argued that introducing more Fe^{3+} at Si^{4+} sites in the glass network leads to a decrease in the angle of T–O–T linkage which results in a bond length increase. As a result, in the Fe-albite sample with a higher Si/Fe ratio, the frequency of the antisymmetric vibrations of BOs increases (HF band shifts to higher frequencies).

The fraction of iron that exists as Fe^{2+} acts as network modifier (similar to Mg^{2+} and Ca^{2+} in silicate glasses), resulting in network depolymerization. Moreover, even though Fe^{3+} is normally a tetrahedral network former, it can also act as octahedral network modifier, even when other cations can compensate the charge balance for its tetrahedral coordination (Mysen and Richet, 2005). Therefore, while in some papers the three compositions studied here are assumed to have “fully polymerized” network, a fraction of their oxygens is actually non-bridging (unlike the Al equivalent compositions), due to some Fe acting as network modifier. Even though some Fe crystallizes into magnetite during NaFeSiO_4 quench, the Si/Fe ratio in the glass still remains lower than that of $\text{NaFeSi}_2\text{O}_6$ and $\text{NaFeSi}_3\text{O}_8$, because the formed magnetite is only ~7.5 wt% (Table 2). The estimated residual glass composition for the Fe-nepheline as-quenched glass is $\sim\text{NaFe}_{0.84}\text{SiO}_x$.

Changes on heat treatment

Upon the heat-treatment of Fe-nepheline at 775°C for 7 h, the magnetite phase (spinel, Fe_3O_4) oxidizes to hematite (Fe_2O_3), and some Fe may be rejected from the glass into hematite, whereas a high fraction of the glass remains amorphous. With longer heat-treatment times at higher temperature, as discussed in (Ahmadzadeh et al., 2017), the amorphous phase can reject more Fe, creating additional hematite.

For the $\text{NaFeSi}_2\text{O}_6$ composition, on the other hand, a portion of the glass transforms to the aegirine phase during heat treatment at 900°C for 24 h. Trace amounts of hematite are also formed.

It is interesting to note that even though the glass extensively forms aegirine crystals after the heat-treatment, no noticeable crystallization peak is observed in its DTA curve, while the aegirine melting peak is observed. Most likely, some aegirine crystals have formed in the DTA sample during non-isothermal heating, though not enough to show up as an exothermic peak. This is likely because the formation of aegirine is kinetically controlled by the relatively high heating rate of 10 °C min⁻¹ in the thermal analysis, as also suggested by other studies (Plaisted et al., 2000; Vienna et al., 1996).

The Mössbauer spectrum of the crystallized aegirine (Figure 2-d) confirms the presence of ^[6]Fe³⁺ in the crystal along with some ^[4]Fe³⁺ of the glass. The XAS pre-edge centroid of the crystallized aegirine (NaFeSi₂O₆_900°C-24h) shown in Figure 3-c exhibits a shift to higher energies (+0.2 eV), combined with a shift to lower intensities, compared to those of the glasses. Comparing to the Mössbauer data (Figure 2), this observed pre-edge shift agrees with the conversion to ~100% Fe³⁺ upon crystallization, considerable amounts of ^[6]Fe³⁺ in the aegirine crystal, and some remaining ^[4]Fe³⁺ in the residual glass. This change can be seen qualitatively in comparing the whole XANES spectra (Figure 3-a) of the natural aegirine standard, the NaFeSi₂O₆_900C-24h (crystallized) and the NaFeSi₂O₆_AQ (glass), with the intensity of the pre-edge features increasing visibly in this series, respectively.

In the case of NaFeSi₃O₈, due to high SiO₂ content and hence strong glass forming ability, the glass does not crystallize during heat-treatment at 1000°C for 24 h, even though some Fe leaves the glass as a small fraction of hematite. This composition can crystallize aegirine in addition to hematite upon prolonged isothermal heat-treatment times at lower temperatures (i.e., 900°C for 72 h).

It was previously shown that $\text{NaFeSi}_2\text{O}_6$ and $\text{NaFeSi}_3\text{O}_8$ glasses do not form the respective silicate crystals upon slow cooling of the melts ($5\text{ }^\circ\text{C min}^{-1}$ from 1500 to 600°C followed by rapid quench) (Marcial and McCloy, 2019). However, at least for aegirine, the phase has been observed to crystallize heterogeneously (surface crystallization) in non-isochemical compositions following a long induction for nucleation, confirming that formation of aegirine is controlled kinetically (Plaisted et al., 2000; Vienna et al., 1996). In the case of Fe-albite, the conditions for nucleation of the crystalline phase, if it exists, may mimic that of albite, where the nucleation time is extremely long and the temperature of maximum nucleation is well below T_g in a region of high viscosity, making albite glass almost impossible to crystallize in a water-free, seed-free experiment (Zanotto and Cassar, 2017).

Related mineral systems

The Al^{3+} equivalents of the compositions studied here, i.e., NaAlSiO_4 (nepheline or carnegieite), $\text{NaAlSi}_2\text{O}_6$ (jadeite), and $\text{NaAlSi}_3\text{O}_8$ (albite) can form distinct crystalline phases and are well-studied rock-forming minerals (Deer et al., 2004; Marcial et al., 2016; Marcial and McCloy, 2019; Palmer, 1994). Al^{3+} , for which we substituted Fe^{3+} , is tetrahedrally coordinated by oxygen atoms in nepheline and albite structures, while octahedrally coordinated in jadeite. Substitution of all Al^{3+} by Fe^{3+} did not form the same crystal structure for nepheline and albite, whereas $\text{NaFe}^{3+}\text{Si}_2\text{O}_6$ forms isomorphous crystals to $\text{NaAl}^{3+}\text{Si}_2\text{O}_6$. Nonetheless, it was shown in (Ahmadzadeh et al., 2017) that the nepheline structure can incorporate significant amounts of Fe^{3+} (up to $x=0.37$ in $\text{NaAl}_{(1-x)}\text{Fe}_x\text{SiO}_4$) in Al^{3+} sites. Moreover, Bailey and Schairer (Bailey and Schairer, 1963; Bailey and Schairer, 1966) have observed that albite can also accommodate a limited amount of iron in its structure, likely in Al sites, though most Fe found in feldspars is in impurities of magnetite and hematite (Montiel-Anaya and Franco, 2019).

Comparison with the other alkali oxide-Fe₂O₃-SiO₂ systems is warranted. In the K₂O-Fe₂O₃-SiO₂ system, the K analogues of all these three compounds (i.e. KFeSiO₄, KFeSi₂O₆, and KFeSi₃O₈) exist as crystalline phases (Faust, 1936; Lange et al., 1986). In fact, not only iron-leucite (KFeSi₂O₆) (Bell and Henderson, 1994), but also iron-kalsilite (KFeSiO₄) (Bentzen, 1983) and iron-orthoclase/ ferri-sanidine (KFeSi₃O₈) (Lebedeva et al., 2003; Shchipalkina et al., 2019) are isomorphous to their Al equivalents, and Fe³⁺ is tetrahedrally coordinated in all three compounds. The Li equivalent of aegirine (LiFeSi₂O₆), known as Li-aegirine, crystallizes in the same crystal structure as spodumene (LiAlSi₂O₆) and aegirine (NaFeSi₂O₆), i.e., monoclinic structure with space group *C2/c*, with ^[6]Fe³⁺ (Lottermoser et al., 1998; Zhang et al., 2002). However, this phase is not reported as a natural mineral. LiFeSiO₄ has been reported, but is not known as a natural mineral (Honma et al., 2012; Nyttén et al., 2006). To our knowledge, LiFeSi₃O₈ has only been calculated but not experimentally reported (Persson, 2014).

It is notable that the coordination of Fe³⁺ has been shown to be particularly strongly influenced by the nature of the alkali cation in some silicate glasses, wherein ^[CN]Fe³⁺ decreases (from 6 (Li) to 4 (K)) with increasing alkali ionic radius (Bingham et al., 2014). This is qualitatively consistent with the coordination behavior of Fe³⁺ in the crystalline systems described above. Even with the same coordination number, the ionic size may still influence the stability of a given crystal structure, such as for alkali-Fe³⁺-feldspar, where the distortion of the Na environment due to its smaller ionic size is less favorable for the feldspar structure than K (Shchipalkina et al., 2019).

IMPLICATIONS

Three sodium iron silicate compositions (NaFeSiO_4 – Fe-nepheline, $\text{NaFeSi}_2\text{O}_6$ – aegirine, $\text{NaFeSi}_3\text{O}_8$ – Fe-albite) have been studied. The high- SiO_2 compositions (aegirine and Fe-albite with $\text{SiO}_2 > 50$ wt%) can readily form glass upon quenching, whereas Fe-nepheline crystallizes magnetite even at relatively fast quench rates because of its lower Si/Fe ratio. In the glasses, although there is some Fe^{2+} (<20%, depending on the composition), most of the iron occurs as 4-coordinated Fe^{3+} cations. However, when Fe crystallizes as the sodium iron silicate mineral (i.e., aegirine) upon isothermal heat-treatment, it arranges as Fe^{3+} octahedra (6-coordinated). It was found that analysis of pre-edge XANES features is less sensitive than Mössbauer for the study of Fe redox and coordination in such compositions where $\text{Fe}^{3+}/\sum\text{Fe}$ does not vary significantly. The as-quenched glasses show similar Raman spectra with intense low-frequency (200-600 cm^{-1}) and high-frequency (800-1200 cm^{-1}) envelopes, and systematic changes of their frequency and relative intensity based on their changing Si/Fe ratio. Moreover, the thermal analysis of these glass reveals an increase in the glass transition temperature from $T_g=471^\circ\text{C}$ in NaFeSiO_4 (Si/Fe=1) to $T_g\sim 521^\circ\text{C}$ in $\text{NaFeSi}_3\text{O}_8$ (Si/Fe=3), due to the stronger Si-O bonds substituting for Fe-O bonds.

The study of these simplified compositions can help understand the potential phases that may crystallize within high-Fe nuclear waste glasses, which can affect their aqueous alteration behavior (Deshkar et al., 2019). It is shown that, in $\text{NaFeSi}_x\text{O}_{(2x+2)}$ type compositions, Fe crystallizes as iron spinel (i.e., magnetite) upon quench when $x=1$ (even at high quench rates); the melt can readily form a glass when $x\geq 2$; and the glass can hardly crystallize when $x\geq 3$. Increasing the Si/Fe ratio was found to increase the Fe^{2+} fraction, consistent with known models, which has a network modifying role. The correlation between Si/Fe ratio and Fe oxidation state in such glasses, is important for geosciences and high-Fe nuclear waste management, as it can influence

the melt polymerization, and as shown here, its crystallization behavior. Details of Fe chemistry are also important for nuclear waste vitrification processes, as the redox strongly influences foaming behavior and melt rate (Pokorny and Hrma, 2014). For a full understanding, future studies should be conducted with deliberate control of the Fe oxidation state of the starting glass, for these same compositions, in order to obtain a more complete understanding of the role of Fe conformation and Fe content on network topology and resulting thermal properties and viscosity.

ACKNOWLEDGEMENTS

This research was supported by the Department of Energy Waste Treatment and Immobilization Plant Federal Project Office, contract numbers DE-EM002904 and 89304017CEM000001, under the direction of Dr. Albert A. Kruger. A portion of this research used 6-BM of the National Synchrotron Light Source II (NSLSII), a US DOE OS user facility operated for the DOE OS by Brookhaven National Laboratory (BNL) under contract DE-SC0012704. This work was, in part, performed in the HADES / MIDAS facility at the University of Sheffield, established with financial support of the Department for Business, Energy & Industrial Strategy and Engineering and Physical Sciences Research Council (EPSRC) under grant EP/T011424/1. The UK portion of the research was sponsored, in part, by the UK Engineering and Physical Sciences Research Council under grants EP/N017870/1 and EP/S01019X/1. The authors would like to thank Daniel Neuville from the Institut de Physique du Globe de Paris (IPGP) for help with Raman spectroscopy measurements and interpretation.

REFERENCES CITED

- Ahmadzadeh, M., Marcial, J., and McCloy, J. (2017) Crystallization of iron-containing sodium aluminosilicate glasses in the NaAlSiO₄-NaFeSiO₄ join. *Journal of Geophysical Research: Solid Earth*, 122, 2504-2524.
- Ahmadzadeh, M., Olds, T.A., Scrimshire, A., Bingham, P.A., and McCloy, J.S. (2018) Structure and properties of Na₅FeSi₄O₁₂ crystallized from 5Na₂O-Fe₂O₃-8SiO₂ glass. *Acta Crystallographica Section C*, 74, 1595-1602.
- Baert, K., Meulebroeck, W., Wouters, H., Cosyns, P., Nys, K., Thienpont, H., and Terryn, H. (2011) Using Raman spectroscopy as a tool for the detection of iron in glass. *Journal of Raman Spectroscopy*, 42, 1789-1795.
- Bailey, D.K., and Schairer, J.F. (1963) Crystallization of the rock-forming silicates in the system Na₂O-Fe₂O₃-Al₂O₃-SiO₂ at 1 atmosphere. *Carnegie Institution Wash. Year Book* 62, 124-131.
- Bailey, D.K., and Schairer, J.F. (1966) The System Na₂O-Al₂O₃-Fe₂O₃-SiO₂ at 1 Atmosphere, and the Petrogenesis of Alkaline Rocks. *Journal of Petrology*, 7, 114-170.
- Baum, E., Treutmann, W., Behruzi, M., Lottermoser, W., and Amthauer, G. (1988) Structural and magnetic properties of the clinopyroxenes NaFeSi₂O₆ and LiFeSi₂O₆. *Zeitschrift für Kristallographie - Crystalline Materials*, 183, 273.
- Bell, A.M.T., and Henderson, C.M.B. (1994) Rietveld refinement of the structures of dry-synthesized MFe^{III}Si₂O₆ leucites (M= K, Rb, Cs) by synchrotron X-ray powder diffraction. *Acta Crystallographica C*, 50, 1531-1536.
- Bentzen, J.J. (1983) Three Crystalline Polymorphs of KFeSiO₄, Potassium Ferrisilicate. *Journal of the American Ceramic Society*, 66, 475-479.
- Bingham, P.A., Hannant, O.M., Reeves-McLaren, N., Stennett, M.C., and Hand, R.J. (2014) Selective behaviour of dilute Fe³⁺ ions in silicate glasses: an Fe K-edge EXAFS and XANES study. *Journal of Non-Crystalline Solids*, 387, 47-56.
- Bowen, N.L., Schairer, J.F., and Willems, H.W.V. (1930) The ternary system; Na₂SiO₃-Fe₂O₃-SiO₂. *American Journal of Science, Series 5 Vol. 20*, 405-455.
- Bychkov, A.M., Borisov, A., Khramov, D.A., and Urusov, V. (1993) Change in the immediate environment of Fe atoms during the melting of minerals (review). *Geochemistry International*, 30, 1-25.
- Cameron, M., Sueno, S., Prewitt, C., and Papike, J. (1973) High-Temperature Crystal Chemistry of Acmite, Diopside, Hedenbergite, Jadeite, Spodumene, and Ureyite. *American Mineralogist*, 58, 594-618.
- Clark, J.R., Appleman, D.E., and Papike, J.J. (1969) Crystal-chemical characterization of clinopyroxenes based on eight new structure refinements. *Mineralogical Society of America Special paper*, 2, 31-50.
- Cochain, B., Neuville, D.R., Henderson, G.S., McCammon, C.A., Pinet, O., and Richet, P. (2012) Effects of the Iron Content and Redox State on the Structure of Sodium Borosilicate Glasses: A Raman, Mössbauer and Boron K-Edge XANES Spectroscopy Study. *Journal of the American Ceramic Society*, 95, 962-971.
- Cochain, B., Neuville, D.R., Richet, P., Henderson, G.S., and Pinet, O. (2008) Determination of iron redox ratio in borosilicate glasses and melts from Raman spectra. *Atalante 2008: Nuclear fuel cycle for a sustainable future*, p. O4-11, France.

- Cottrell, E., Kelley, K.A., Lanzirrotti, A., and Fischer, R.A. (2009) High-precision determination of iron oxidation state in silicate glasses using XANES. *Chemical Geology*, 268, 167-179.
- Deer, W.A., Howie, R.A., Wise, W.S., and Zussman, J. (2004) Framework silicates: silica minerals, feldspathoids and the zeolites. *Rock-forming minerals. The Geological Society, Geological Society Publishing House, London.*
- Deer, W.A., Howie, R.A., and Zussman, J. (1992) *An introduction to rock-forming minerals.* Longman, Essex, England.
- Deshkar, A., Ahmadzadeh, M., Scrimshire, A., Han, E., Bingham, P.A., Guillen, D., McCloy, J., and Goel, A. (2019) Crystallization behavior of iron- and boron-containing nepheline ($\text{Na}_2\text{O}\cdot\text{Al}_2\text{O}_3\cdot 2\text{SiO}_2$) based model high-level nuclear waste glasses. *Journal of the American Ceramic Society*, 102, 1101-1121.
- Di Genova, D., Vasseur, J., Hess, K.-U., Neuville, D.R., and Dingwell, D.B. (2017) Effect of oxygen fugacity on the glass transition, viscosity and structure of silica- and iron-rich magmatic melts. *Journal of Non-Crystalline Solids*, 470, 78-85.
- Di Muro, A., Métrich, N., Mercier, M., Giordano, D., Massare, D., and Montagnac, G. (2009) Micro-Raman determination of iron redox state in dry natural glasses: Application to peralkaline rhyolites and basalts. *Chemical Geology*, 259, 78-88.
- Dyar, M.D. (1985) A review of Moessbauer data on inorganic glasses; the effects of composition on iron valency and coordination. *American Mineralogist*, 70, 304-316.
- Dyar, M.D., Agresti, D.G., Schaefer, M.W., Grant, C.A., and Sklute, E.C. (2006) Mössbauer spectroscopy of earth and planetary materials. *Annual Review of Earth and Planetary Sciences*, 34, 83-125.
- Farges, F., Lefrère, Y., Rossano, S., Berthereau, A., Calas, G., and Brown Jr, G.E. (2004) The effect of redox state on the local structural environment of iron in silicate glasses: a combined XAFS spectroscopy, molecular dynamics, and bond valence study. *Journal of Non-Crystalline Solids*, 344, 176-188.
- Farges, F., Rossano, S., Lefrère, Y., Wilke, M., and G. E. Brown, J. (2005) Iron in silicate glasses: a systematic analysis of pre-edge, XANES and EXAFS features. *Physica Scripta*, 2005, 957.
- Faust, G.T. (1936) The Fusion Relations of Iron-Orthoclase. *American Mineralogist*, 21, 735-763.
- Fiege, A., Ruprecht, P., Simon, A.C., Bell, A.S., Göttlicher, J., Newville, M., Lanzirrotti, T., and Moore, G. (2017) Calibration of Fe XANES for high-precision determination of Fe oxidation state in glasses: Comparison of new and existing results obtained at different synchrotron radiation sources. *American Mineralogist*, 102, 369-380.
- Fleet, M.E., Herzberg, C.T., Henderson, G.S., Crozier, E.D., Osborne, M.D., and Scarfe, C.M. (1984) Coordination of Fe, Ga and Ge in high pressure glasses by Mössbauer, Raman and X-ray absorption spectroscopy, and geological implications. *Geochimica et Cosmochimica Acta*, 48, 1455-1466.
- Forder, S.D., Bingham, P.A., McGann, O.J., Stennett, M.C., and Hyatt, N.C. (2013) Mössbauer studies of materials used to immobilise industrial wastes. *Hyperfine Interactions*, 217, 83-90.
- Galoisy, L., Calas, G., and Arrio, M.A. (2001) High-resolution XANES spectra of iron in minerals and glasses: structural information from the pre-edge region. *Chemical Geology*, 174, 307-319.

- Henderson, G.S., Fleet, M.E., and Bancroft, G.M. (1984) An x-ray scattering study of vitreous KFeSi_3O_8 and $\text{NaFeSi}_3\text{O}_8$ and reinvestigation of vitreous SiO_2 using quasi-crystalline modelling. *Journal of Non-Crystalline Solids*, 68, 333-349.
- Honma, T., Togashi, T., and Komatsu, T. (2012) Spinel-type crystals based on LiFeSiO_4 with high electrical conductivity for lithium ion battery formed by melt-quenching method. *Journal of the Ceramic Society of Japan*, 120, 93-97.
- Hrma, P.R., Vienna, J.D., Mika, M., Crum, J.V., and Piepel, G.F. (1999) Liquidus Temperature Data for DWPF Glass, p. Medium: ED; Size: 72 pages. PNNL-11790, Pacific Northwest National Lab., Richland, WA (US).
- Jackson, W.E., Farges, F., Yeager, M., Mabrouk, P.A., Rossano, S., Waychunas, G.A., Solomon, E.I., and Brown Jr, G.E. (2005) Multi-spectroscopic study of Fe(II) in silicate glasses: Implications for the coordination environment of Fe(II) in silicate melts. *Geochimica et Cosmochimica Acta*, 69, 4315-4332.
- Jantzen, C., and Edwards, T. (2015) Product/Process (P/P) Models For The Defense Waste Processing Facility (DWPF): Model Ranges And Validation Ranges For Future Processing, p. Medium: ED. SRNL-STI-2014-00320, Savannah River National Laboratory, Aiken, SC.
- Jantzen, C.M. (2011) Development of glass matrices for high level radioactive wastes. In M.I. Ojovan, Ed. *Handbook of Advanced Radioactive Waste Conditioning Technologies*, p. 230-292. Woodhead Publishing.
- Jantzen, C.M., and Bickford, D.F. (1984) Leaching of Devitrified Glass Containing Simulated SRP Nuclear Waste. *MRS Proceedings*, 44, 135.
- Jantzen, C.M., Bickford, D.F., and Karraker, D.G. (1984) Time-Temperature-Transformation [TTT] Kinetics in SRL Waste Glass. In G.G. Wicks, and W.A. Ross, Eds. *Advances in Ceramics* 85, 85, p. 30-38. American Ceramic Society, Columbus, OH.
- Jantzen, C.M., and Brown, K.G. (2007) Predicting the spinel–nepheline liquidus for application to nuclear waste glass processing. Part II: quasicrystalline freezing point depression model. *Journal of the American Ceramic Society*, 90, 1880-1891.
- Jantzen, C.M., Brown, K.G., and Pickett, J.B. (2010) Durable glass for thousands of years. *International Journal of Applied Glass Science*, 1, 38-62.
- Jayasuriya, K.D., O'Neill, H.S.C., Berry, A.J., and Campbell, S.J. (2004) A Mössbauer study of the oxidation state of Fe in silicate melts. *American Mineralogist*, 89, 1597-1609.
- Jeoung, J.-S., Poisl, W.H., Weinberg, M.C., Smith, G.L., and Li, H. (2001) Effect of Oxidation State of Iron on Phase Separation in Sodium Silicate Glasses. *Journal of the American Ceramic Society*, 84, 1859-1864.
- Kim, D.S., Hrma, P., Smith, D.E., and Schweiger, M.J. (1994) Crystallization in Simulated Glasses from Hanford High-Level Nuclear Waste Composition Range. In G.B. Mellinger, Ed. *Ceramic Transactions*, 39, p. 179-189. American Ceramic Society, Westerville, OH.
- Kim, D.S., Schweiger, M.J., Rodriguez, C.P., Lepry, W.C., Lang, J.B., Crum, J.D., Vienna, J.D., Johnson, F.C., Marra, J.C., and Peeler, D.K. (2011) Formulation and characterization of waste glasses with varying processing temperature. PNNL-20774, Pacific Northwest National Laboratory, Richland, WA.
- Komatsu, T., and Soga, N. (1980) ESR and Mössbauer studies of crystallization process of sodium iron silicate glass. *The Journal of Chemical Physics*, 72, 1781-1785.

- Kruger, A.A., Pegg, I.L., Chaudhuri, M., Gong, W., Gan, H., Matlack, K.S., Bardakci, T., and Kot, W. (2013) Final report - melt rate enhancement for high aluminum HLW glass formulation. VSL-08R1360-1, Hanford Site (HNF), Richland, WA.
- Lange, R.A., Carmichael, I.S.E., and Stebbins Jonathan, F. (1986) Phase transitions in leucite (KAlSi_2O_6), orthorhombic KAlSiO_4 , and their iron analogues (KFeSi_2O_6 , KFeSiO_4). *American Mineralogist*, 71, 937-945.
- Larsen, I.M. (1976) Clinopyroxenes and Coexisting Mafic Minerals from the Alkaline Ilímaussaq Intrusion, South Greenland. *Journal of Petrology*, 17, 258-290.
- Lebedeva, Y.S., Pushcharovsky, D.Y., Pasero, M., Merlino, S., Kashaev, A.A., Taroev, V.K., Goettlicher, J., Kroll, H., Pentinghaus, H., Suvorova, L.F., Wulf-Bernodat, H., and Lashkevich, V.V. (2003) Synthesis and crystal structure of low ferrialuminosilicate sanidine. *Crystallography Reports*, 48, 919-924.
- Liu, Q., and Lange, R.A. (2006) The partial molar volume of Fe_2O_3 in alkali silicate melts: Evidence for an average Fe^{3+} coordination number near five. *American Mineralogist*, 91, 385-393.
- Long, D.A. (1977) Raman spectroscopy. McGraw-Hill, New York.
- Lottermoser, W., Redhammer, G., Forcher, K., Amthauer, G., Paulus, W., André, G., and Treutmann, W. (1998) Single crystal Mössbauer and neutron powder diffraction measurements on the synthetic clinopyroxene Li-acmite $\text{LiFeSi}_2\text{O}_6$. *Zeitschrift für Kristallographie - Crystalline Materials*, 213, 101-107.
- Luo, Y.-R., and Kerr, J.A. (2006) Bond Dissociation Energies. In D.R. Lide, Ed. *CRC Handbook of Chemistry and Physics*, p. 9-54-9-59. Taylor and Francis, Boca Raton.
- Magnien, V., Neuville, D.R., Cormier, L., Roux, J., Hazemann, J.L., Pinet, O., and Richet, P. (2006) Kinetics of iron redox reactions in silicate liquids: A high-temperature X-ray absorption and Raman spectroscopy study. *Journal of Nuclear Materials*, 352, 190-195.
- Marcial, J., Ahmadzadeh, M., and McCloy, J.S. (2016) Effect of Li, Fe, and B Addition on the Crystallization Behavior of Sodium Aluminosilicate Glasses as Analogues for Hanford High Level Waste Glasses. *MRS Advances*, 1-7.
- Marcial, J., and McCloy, J. (2019) Role of short range order on crystallization of tectosilicate glasses: A diffraction study. *Journal of Non-Crystalline Solids*, 505, 131-143.
- Montiel-Anaya, J.A., and Franco, V. (2019) FORC study of the ferromagnetic impurities in Na and K feldspars of “El Realejo” mine. *AIP Advances*, 9, 035038.
- Mysen, B.O., and Richet, P. (2005) *Silicate glasses and melts: properties and structure*. Elsevier, Amsterdam.
- Mysen, B.O., Seifert, F., and Virgo, D. (1980) Structure and redox equilibria of iron-bearing silicate melts. *American Mineralogist*, 65, 867-884.
- Nestola, F., Tribaudino, M., Boffa Ballaran, T., Liebske, C., and Bruno, M. (2007) The crystal structure of pyroxenes along the jadeite–hedenbergite and jadeite–aegirine joins. *American Mineralogist*, 92, 1492-1501.
- Nytén, A., Kamali, S., Häggström, L., Gustafsson, T., and Thomas, J.O. (2006) The lithium extraction/insertion mechanism in $\text{Li}_2\text{FeSiO}_4$. *Journal of Materials Chemistry*, 16, 2266-2272.
- Oh, S.J., Cook, D.C., and Townsend, H.E. (1998) Characterization of iron oxides commonly formed as corrosion products on steel. *Hyperfine Interactions*, 112, 59-66.
- Palmer, D.C. (1994) Stuffed derivatives of the silica polymorphs. *Reviews in Mineralogy and Geochemistry*, 29, 83-122.

- Persson, K. (2014) Materials Data on $\text{LiFeSi}_3\text{O}_8$ (SG:2) by Materials Project. ; LBNL Materials Project; Lawrence Berkeley National Lab. (LBNL), Berkeley, CA (United States).
- Plaisted, T., Mo, F., Wilson, B., Young, C., and Hrma, P. (2000) Surface Crystallization and Composition of Spinel and Acmite in High-Level Waste Glass. In D.R. Spearing, G.L. Smith, and R.L. Putnam, Eds. *Ceramics Transactions*, 119, p. 317-325. American Ceramic Society, Westerville, OH.
- Pokorny, R., and Hrma, P. (2014) Model for the conversion of nuclear waste melter feed to glass. *Journal of Nuclear Materials*, 445, 190-199.
- Rancourt, D. (1998) Recoil Mössbauer Spectral Analysis Software. Ottawa: Intelligent Scientific Applications Inc.
- Sack, R.O., Carmichael, I.S.E., Rivers, M., and Ghiorso, M.S. (1980) Ferric-ferrous equilibria in natural silicate liquids at 1 bar. *Contributions to Mineralogy and Petrology*, 75, 369-376.
- Shchipalkina, N.V., Pekov, I.V., Britvin, S.N., Koshlyakova, N.N., Vigasina, M.F., and Sidorov, E.G. (2019) A New Mineral Ferrisanidine, $\text{K}[\text{Fe}^{3+}\text{Si}_3\text{O}_8]$, the First Natural Feldspar with Species-Defining Iron. *Minerals*, 9, 770.
- Vienna, J.D., Hrma, P., and Smith, D.E. (1996) Isothermal Crystallization Kinetics in Simulated High-Level Nuclear Waste Glass. *Proc. of MRS*, 465, p. 17. Cambridge University Press.
- Wang, Z., Cooney, T.F., and Sharma, S.K. (1993) High temperature structural investigation of $\text{Na}_2\text{O} \cdot 0.5\text{Fe}_2\text{O}_3 \cdot 3\text{SiO}_2$ and $\text{Na}_2\text{O} \cdot \text{FeO} \cdot 3\text{SiO}_2$ melts and glasses. *Contributions to Mineralogy and Petrology*, 115, 112-122.
- Wang, Z., Cooney, T.F., and Sharma, S.K. (1995) In situ structural investigation of iron-containing silicate liquids and glasses. *Geochimica et Cosmochimica Acta*, 59, 1571-1577.
- Weaver, J.L., Wall, N.A., and McCloy, J.S. (2015) Wet chemical and UV-Vis spectrometric iron speciation in quenched low and intermediate level nuclear waste glasses. *MRS Proceedings*, 1744, 93-100.
- Weigel, C., Cormier, L., Calas, G., Galoisy, L., and Bowron, D.T. (2008a) Intermediate-range order in the silicate network glasses $\text{NaFe}_x\text{Al}_{1-x}\text{Si}_2\text{O}_6$ ($x=0,0.5,0.8,1$): A neutron diffraction and empirical potential structure refinement modeling investigation. *Physical Review B*, 78, 064202.
- Weigel, C., Cormier, L., Calas, G., Galoisy, L., and Bowron, D.T. (2008b) Nature and distribution of iron sites in a sodium silicate glass investigated by neutron diffraction and EPSR simulation. *Journal of Non-Crystalline Solids*, 354, 5378-5385.
- Weigel, C., Cormier, L., Galoisy, L., Calas, G., Bowron, D., and Beuneu, B. (2006) Determination of Fe^{3+} sites in a $\text{NaFeSi}_2\text{O}_6$ glass by neutron diffraction with isotopic substitution coupled with numerical simulation. *Applied Physics Letters*, 89, 141911.
- Wilke, M., Farges, F.o., Petit, P.-E., Brown, G.E., Jr., and Martin, F.o. (2001) Oxidation state and coordination of Fe in minerals: An Fe K-XANES spectroscopic study. *American Mineralogist*, 86, 714-730.
- Wilke, M., Partzsch, G.M., Bernhardt, R., and Lattard, D. (2005) Determination of the iron oxidation state in basaltic glasses using XANES at the K-edge. *Chemical Geology*, 220, 143-161.
- Yamamoto, T. (2008) Assignment of pre-edge peaks in K-edge x-ray absorption spectra of 3d transition metal compounds: electric dipole or quadrupole? *X-Ray Spectrometry*, 37, 572-584.
- Zanotto, E.D., and Cassar, D.R. (2017) The microscopic origin of the extreme glass-forming ability of Albite and B_2O_3 . *Scientific Reports*, 7, 43022.

Zhang, M., Redhammer, G., Salje, E., and Mookherjee, M. (2002) $\text{LiFeSi}_2\text{O}_6$ and $\text{NaFeSi}_2\text{O}_6$ at low temperatures: An infrared spectroscopic study. *Physics and Chemistry of Minerals*, 29, 609-616.

FIGURE CAPTIONS

Figure 1. Room temperature curves of magnetization – M, versus magnetic field – H, for a) as-quenched Fe-nepheline, b) as-quenched aegirine and Fe-albite, and c) heat-treated aegirine samples with maximum applied field of 1.8 T. The insets show the curves with maximum applied field of 0.2 T.

Figure 2. Fitted room temperature ^{57}Fe Mössbauer spectra of as-quenched (AQ) Fe-nepheline (a), Aegirine (b), and Fe-albite (c) samples, along with the crystallized aegirine heat-treated at 900°C for 24 h (d). The black points represent experimental data, blue line is total fit, and magenta lines are fits of individual Fe sites. See the online version of this article for color.

Figure 3. Fe K-edge X-ray absorption data. a) Measured XANES of glasses, crystallized glass, and standards, b) fits of the extracted pre-edge, and c) pre-edge integrated intensity versus centroid position (with respect to Fe foil at 7112 eV). Our measured samples are shown in red, whereas the measured standards are in blue. The same standards reported by Wilke et al (Wilke et al., 2001) are shown in filled black circles with their other reported values in open circles.

Figure 4. Raw (a) and treated (b) Raman spectra of NaFeSiO_4 (Fe-nepheline), $\text{NaFeSi}_2\text{O}_6$ (aegirine), and $\text{NaFeSi}_3\text{O}_8$ (Fe-albite) as-quenched (AQ) samples. The curves are offset along Y axis. The data shown in (b) is Long-corrected (Long, 1977), background-subtracted, and area-normalized.

TABLES

Table 1. Studied sodium iron silicate samples

Sample	Formula	wt% oxides			Melting temp (°C)	Isothermal heat treatment	
		Na ₂ O	Fe ₂ O ₃	SiO ₂		Temp (°C)	Time (h)
Fe-nepheline	NaFeSiO ₄	18.13	46.71	35.15	1500	775	7
Aegirine	NaFeSi ₂ O ₆	13.42	34.56	52.02	1500	900	24
Fe-albite	NaFeSi ₃ O ₈	10.65	27.43	61.92	1500	1000 ^a	24

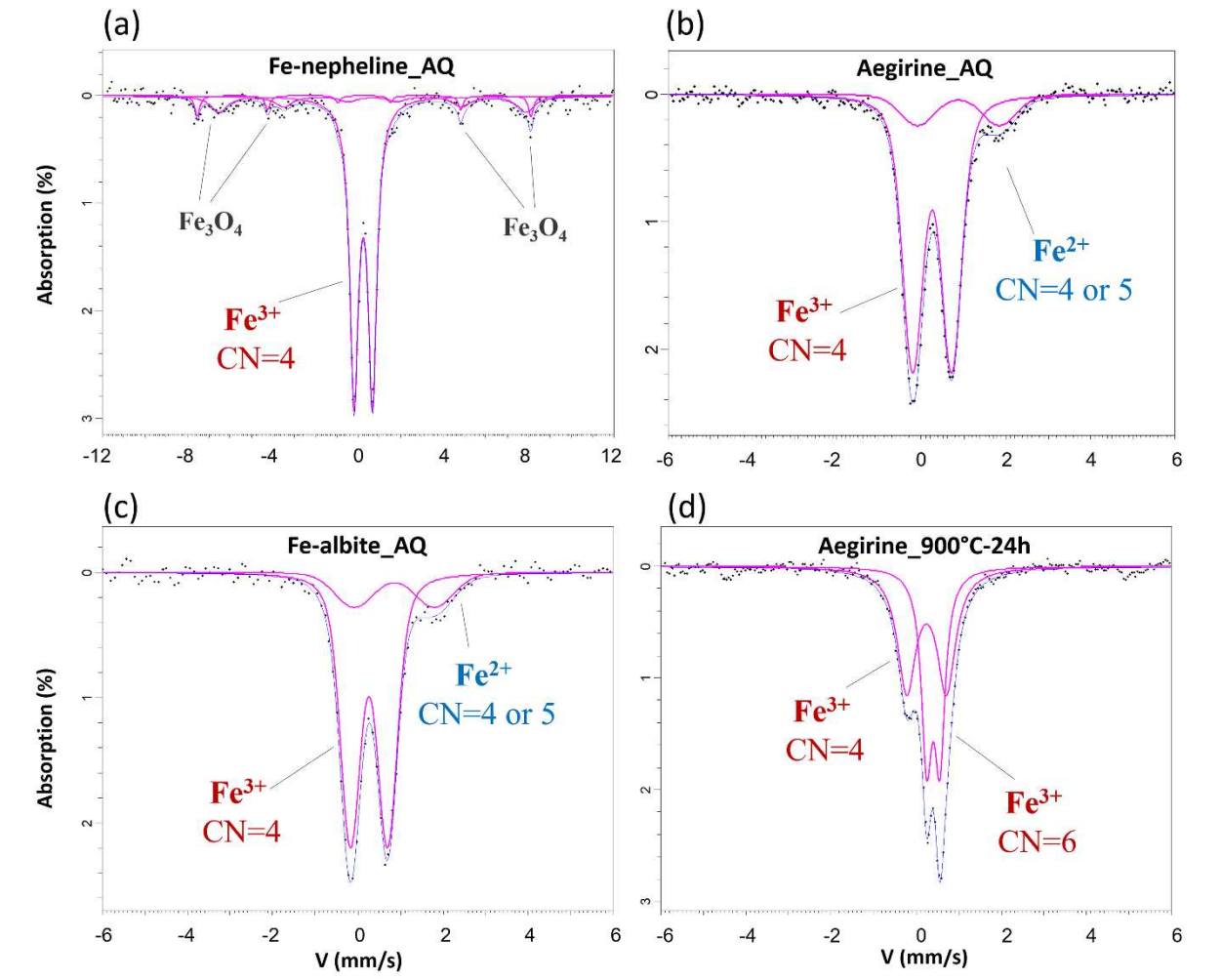
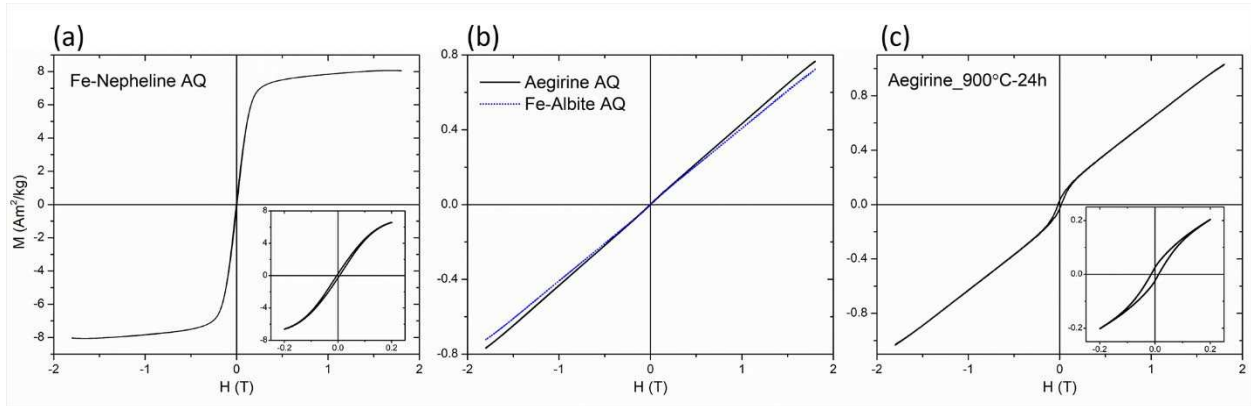
^aThe Fe-albite glass was also heat-treated for longer time (i.e., 72 h) at 900°C to try to crystallize the glass

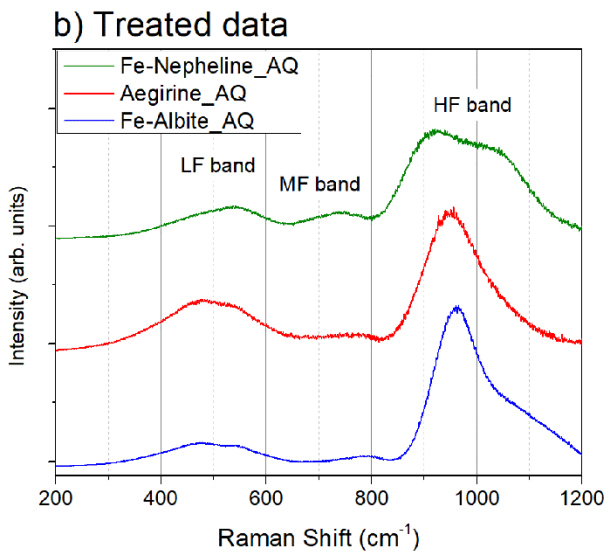
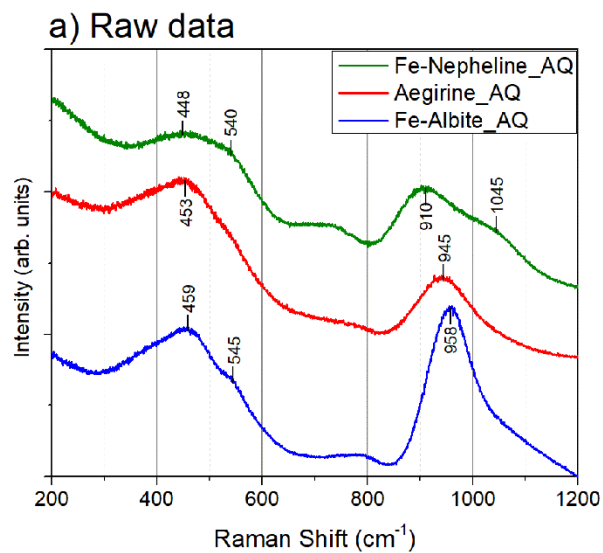
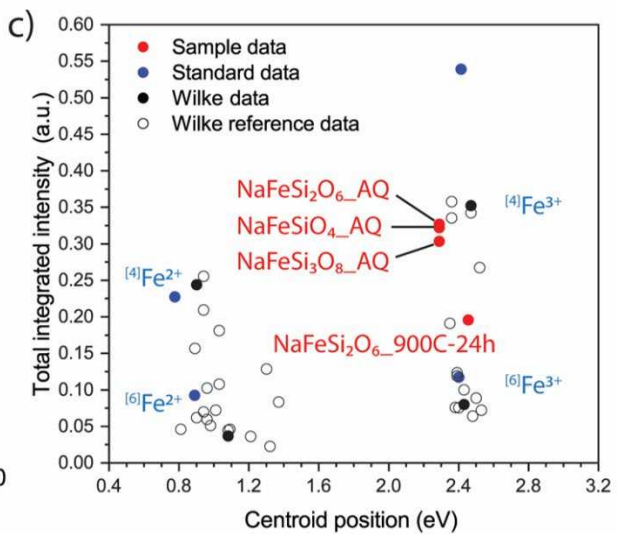
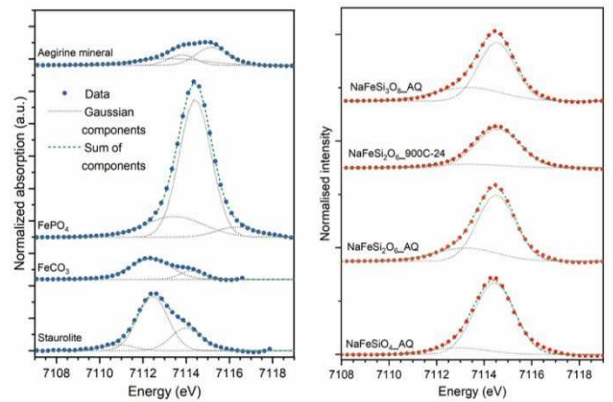
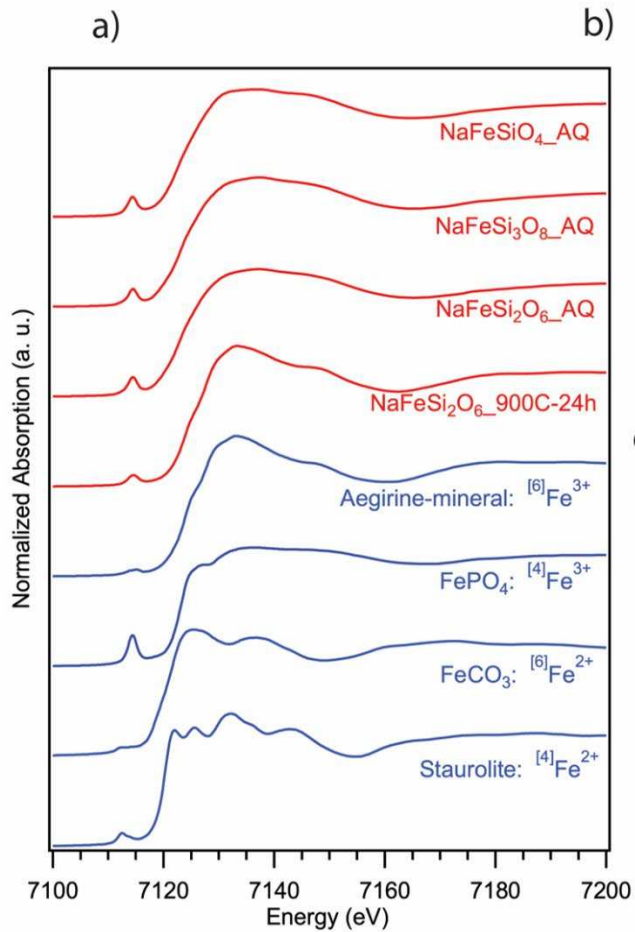
Table 2. Phase analysis of the as-quenched and heat-treated Fe-nepheline, aegirine, and Fe-albite samples, based on XRD and Rietveld refinement results

Composition	Phase Analysis			
	As-quenched (AQ)		Heat-treated (HT)	
	Phases (wt%)	comments	Phases (wt%)	comments
NaFeSiO₄	92.5% Amrph + 7.5% Mgn	Due to low silica content (Si/Fe=1), glass cannot accommodate all Fe easily, and excessive Fe crystallizes as Mgn.	79.2% Amrph + 20.8% Hmt	Mgn further oxidizes to Hmt, and possibly more Fe gets pushed out from glass to Hmt upon heat-treatment in air.
NaFeSi₂O₆	Amrph	Due to higher silica content (Si/Fe=2), glass accommodates all Fe.	7.4% Amrph + 91.4% Ae + 1.2% Hmt	Most of the glass transforms to Ae crystals, while some trace Hmt is observed.
NaFeSi₃O₈	Amrph	Due to high silica content (Si/Fe=3), glass accommodates all Fe.	95.5% Amrph + 4.5% Hmt (HT for 72 h at 900°C crystallizes 19% Ae too)	High silica does not allow the glass to crystallize readily. Only a small fraction of Hmt precipitates. (In case of longer HT time, Ae can crystallize.)

Amrph: amorphous; Mgn: magnetite; Hmt: hematite; Ae: aegirine.

FIGURES





Supplementary information for

Structure of NaFeSiO₄, NaFeSi₂O₆, and NaFeSi₃O₈

glasses and glass-ceramics

Mostafa Ahmadzadeh,^{a,c} Alex Scrimshire,^b Lucy Mottram,^d Martin C. Stennett,^d

Neil C. Hyatt,^d Paul A. Bingham,^b John S. McCloy^{a,c,d,e,*}

^aMaterials Science and Engineering Program, Washington State University, Pullman, WA, 99164, USA

^bMaterials and Engineering Research Institute, Sheffield Hallam University, Sheffield S1 1WB, UK

^cSchool of Mechanical and Materials Engineering, Washington State University, Pullman, WA, 99164,
USA

^dDepartment of Materials Science and Engineering, The University of Sheffield, Sheffield, S1 3JD, UK

^eInstitut de Physique du Globe de Paris, Équipe Géomatériaux, Paris, France

*Corresponding author, E-mail address: john.mccloy@wsu.edu

XRD Patterns

X-ray diffraction patterns for the as-quenched glasses (black) and heat-treated samples (red) are shown in Figure S1.

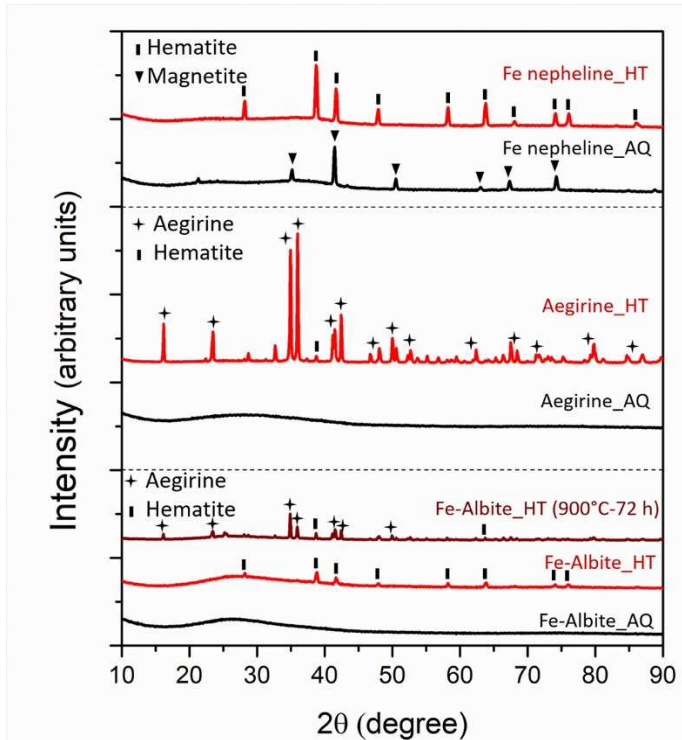


Figure S1. XRD patterns of as-quenched (AQ) and heat-treated (HT) NaFeSiO_4 (Fe-nepheline), $\text{NaFeSi}_2\text{O}_6$ (aegirine), and $\text{NaFeSi}_3\text{O}_8$ (Fe-albite).

Thermal Analysis

The DTA and TGA results of the three as-quenched glasses are presented in Figure S2. The Fe-nepheline glass, unlike the other two compositions, shows additional features (T_1 , T_2 , and T_3) in the range 400-800°C. The $\text{NaFeSi}_2\text{O}_6$ glass shows a sharp endothermic peak at 998°C (on-peak) which is due to the incongruent melting of aegirine with separation of hematite, as discussed in (Bowen et al., 1930). The other two glasses (Fe-nepheline and Fe-albite) do not show any sharp melting point since they remain mostly amorphous during heating and do not form a significant fraction of crystals with well-defined melting temperatures.

For all three studied compositions, the glasses gain less than 0.5% weight on heating to ~ 1100°C, which can be attributed to oxidation of Fe²⁺ to Fe³⁺ during heating (see Mössbauer section). The samples begin losing weight at temperatures >1100°C, which is most likely due to volatilization of Na at elevated temperatures.

The DTA thermograph of this sample shows two exothermic peaks (T₂ and T₃) in the range of 600-800°C. These peaks are attributed to the rejection of more iron from the glass, the presence of magnetite in the as-quenched material, and its transformations at elevated temperatures, including oxidation of magnetite to hematite which is suggested to begin at ~ 575°C and culminate at higher temperatures (Lepp, 1957).

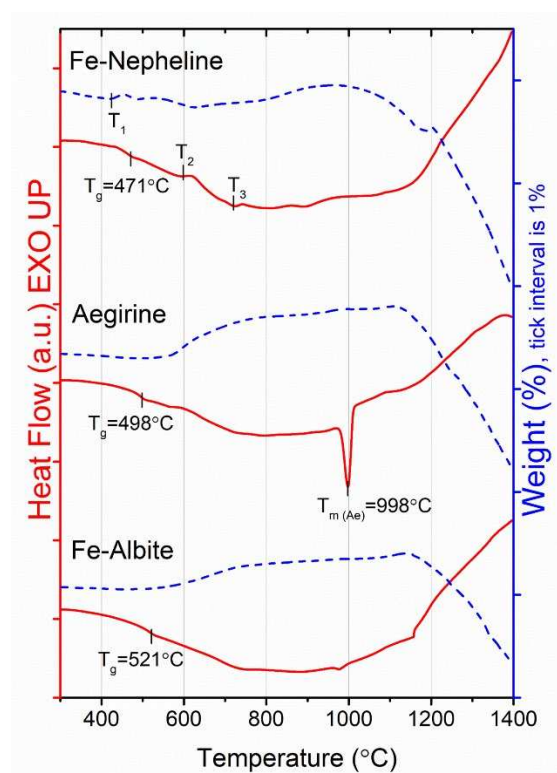


Figure S2. DTA (solid lines) and TGA (dash lines) thermographs for glasses with composition Fe-nepheline (NaFeSiO₄), aegirine (NaFeSi₂O₆), and Fe-albite (NaFeSi₃O₈), heated at 10°C min⁻¹ under constant N₂ flow.

Magnetic Measurements

Such measurements can provide valuable insight into the iron-containing phases (Ahmadzadeh et al., 2017; Deshkar et al., 2017). The Fe-nepheline as-quenched sample reveals a clear saturating magnetic hysteresis loop with relatively high saturation magnetization, due to the presence of the ferrimagnetic magnetite phase within the amorphous glass. The aegirine and Fe-albite as-quenched samples, on the other hand, show a constant increase in the spontaneous magnetization with increasing field, and no magnetic saturation. This paramagnetic behavior is typical for iron-containing amorphous phases (Ahmadzadeh et al., 2017; Smirnov and Tarduno, 2003). Moreover, the as-quenched aegirine sample indicates slightly higher magnetization at a given field as it has a higher concentration of iron, the only present magnetic element, in the paramagnetic glass phase.

The magnetization curve of the heat-treated aegirine sample (900 °C - 24 h), shows contributions from both magnetically-ordered crystals and paramagnetic phase(s). As revealed by XRD results, this sample contains mostly aegirine crystals ($\text{NaFeSi}_2\text{O}_6$), with some hematite (Fe_2O_3) and residual glass. Aegirine is a low-temperature antiferromagnet with a Néel temperature (T_N) of ~ 8 K (Ballet et al., 1989; Baum et al., 1997) above which it becomes paramagnetic. However, pure hematite exhibits canted antiferromagnetism at room temperature with a small magnetization of ~ 0.4 Am²/kg (Dunlop and Özdemir, 1977; Dunlop and Özdemir, 2007), and a relatively high coercive field. Therefore, the observed paramagnetism is from the aegirine phase at room temperature as well as the iron-containing residual glass, whereas the hysteresis behavior is likely due to hematite.

Mössbauer Spectroscopy

The fitted spectral parameters of room temperature Mössbauer spectra of Fe-nepheline, aegirine, and Fe-albite as-quenched samples as well as crystallized aegirine sample, are listed in Table S1.

The values for Fe redox for wet chemical versus Mössbauer methods are listed in Table S2.

Table S1. Fitted Mössbauer parameters of the sodium iron silicate samples obtained from the corresponding spectra. CS is relative to α -Fe foil.

Sample	Signal	CS \pm 0.02 (mm/s)	QS \pm 0.02 (mm/s)	Hyperfine Splitting (T)	Area \pm 2 (%)
Fe-nepheline_AQ	Doublet 1 (Fe ³⁺)	0.24	0.86	-	76.4
	Sextet 1 (magnetite)	0.68	-	44.6	17.3
	Sextet 2 (magnetite)	0.28	-	48.5	6.3
Aegirine_AQ	Doublet 1 (Fe ³⁺)	0.25	0.92	-	84.7
	Doublet 2 (Fe ²⁺)	0.88	1.94	-	15.3
Fe-albite_AQ	Doublet 1 (Fe ³⁺)	0.26	0.87	-	81.2
	Doublet 2 (Fe ²⁺)	0.85	1.88	-	18.8
Aegirine-900°C-24h	Doublet 1 (Fe ³⁺ , CN=4)	0.24	0.93	-	53.9
	Doublet 2 (Fe ³⁺ , CN=6)	0.40	0.31	-	46.1

Table S2. Iron redox values obtained from Mössbauer spectroscopy (xVBF fits) and wet chemistry of as-quenched (AQ) aegirine and Fe-albite samples

		Aegirine_AQ	Fe-albite_AQ
Fe ³⁺ /ΣFe	Mössbauer Spectroscopy	0.847	0.812
	Wet chemistry	Average	0.833
		St. Dev.	0.002
		0.004	

Raman Spectroscopy

While the Raman spectroscopy discussion in this work is purely qualitative, both raw data as well as treated data are reported. Data treatment was carried out by correcting for temperature and excitation line per (Neuvill and Mysen, 1996), then a linear baseline was subtracted, and all spectra were normalized to unit area for comparison. We refer the reader to Di Muro et al. (2009) for discussion of how different methods of treatment and baseline subtraction proposed in the

literature can affect the relative intensity and even the position of Raman bands in various iron silicate glasses.

Low frequency (LF~200-600 cm^{-1}), medium frequency (MF~600-800 cm^{-1}) and high frequency (HF~800-1200 cm^{-1}) envelopes are the three main bands in Raman spectra of most silicate glasses. The LF region in silicate networks is normally assigned to large-scale vibrations of rings of tetrahedra, whereas the HF envelope is conventionally attributed to stretching vibrations of metal-oxygen bonds in individual tetrahedra. The LF envelope, moreover, can potentially reveal some information regarding the inter-tetrahedral angle, the ring arrangement, Si-O⁰ rocking motions, and Si-O-Si bending motions. The intermediate region (MF) is the weakest feature in such glasses and is controversially attributed to various vibrational modes (Di Genova et al., 2016; Di Muro et al., 2009; McMillan, 1984; Mysen et al., 1980; Neuville et al., 2014; Rossano and Mysen, 2012).

X-ray Absorption Spectroscopy

To calibrate the energy scale of the XANES data, the first peak in the first derivative of the reference Fe foil spectrum was set to 7112.00 eV (Bearden and Burr, 1967). Data calibration, normalization and background removal were performed on Athena, from the Demeter system (Ravel and Newville, 2005).

Processing and analysis of the Fe-K edge XANES pre-edge feature were performed using Microsoft Excel® software, as described in (Joseph et al., 2017). First, a spline function was fit to model the contribution of the edge step; this contribution was then subtracted to extract the pre-edge feature. The pre-edge feature was fitted with two Gaussian components (a third component was included dependent on the improvement in goodness of fit), and a total fit was calculated from the sum of these components. A linear least squares refinement was used to optimize the total fit

through adjustment of normalized component height, energy position, and full width at half height. The full width at half height was not constrained, to allow for best agreement between the total fit and the pre-edge feature. The centroid energy position was determined by taking the average centroid energy of the Gaussian components, weighted by intensity. This is a simplified form of the analysis method implemented by Wilke et al. (2001), which used pseudo-Voigt components with a fixed component shape of 50% Gaussian and 50% Lorentzian.

Related mineral systems

The naturally-occurring nepheline contains K in Na sites, $(\text{Na,K})\text{AlSiO}_4$, and is the most abundant member of the feldspathoid group (Edgar, 1984). Nepheline has a hexagonal crystal structure with space group of $P6_3$. Jadeite is an important pyroxene mineral with monoclinic structure and space group $C2/c$, isostructural with aegirine (Nestola et al., 2007; Prewitt and Burnham, 1966). Low albite (completely ordered) is the sodium end member of plagioclase feldspar group which crystallizes in triclinic symmetry with space group of $C\bar{1}$ (Phillips et al., 1989). Crystallization of albite, however, is extremely difficult and slow in the $\text{Na}_2\text{O}-\text{Al}_2\text{O}_3-\text{SiO}_2$ system compared to other feldspars (Bowen and Schairer, 1938; MacKenzie, 1957; Tuttle and Bowen, 1950; Uhlmann et al., 1980; Zanutto and Cassar, 2017), though its hydrothermal synthesis has been reported (Martin, 1969). Figure S3 shows the structures of these three Al phases.

We can infer that Fe^{3+} can entirely substitute Al^{3+} in the sodium aluminosilicate phases in which aluminum is six-coordinated, i.e., form a full-range solid-solution (jadeite – aegirine). As verified by the Mössbauer spectrum for the crystallized aegirine sample (Figure 2d), iron is present as six-coordinated Fe^{3+} in the aegirine phase. However, in the sodium aluminosilicate structures in which Al^{3+} is tetrahedrally coordinated (nepheline and albite), iron can only partially substitute for aluminum.

While similar valence and ionic radii of Fe^{3+} and Al^{3+} lead to similar structural position of these two cations in silicate glasses, this analogy may not always hold true for silicate crystals (Mysen and Richet, 2005; Mysen and Virgo, 1978). As pointed out by Mysen (2005), in silicate crystals, four-coordinated Al^{3+} is common, whereas 4-coordinated Fe^{3+} is rare.

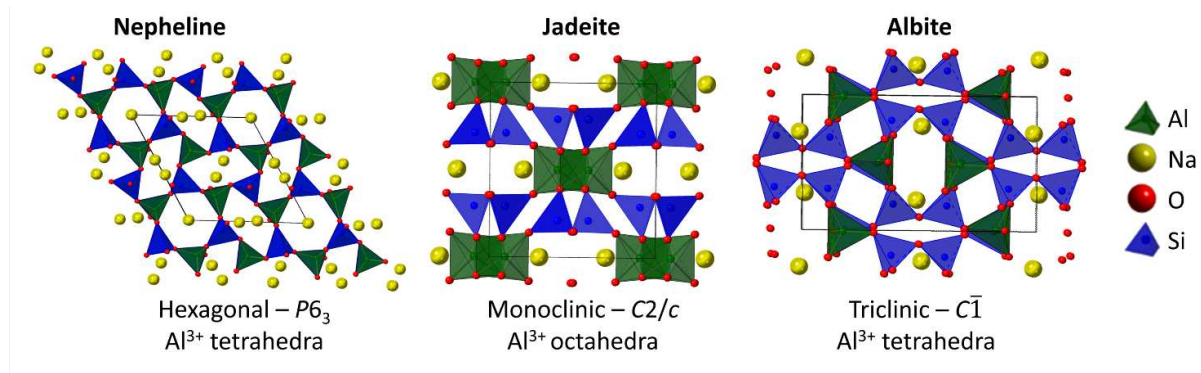


Figure S3. A representation of the crystal structures of nepheline – NaAlSiO_4 (Buerger et al., 1946), jadeite – $\text{NaAlSi}_2\text{O}_6$ (Prewitt and Burnham, 1966), and albite – $\text{NaAlSi}_3\text{O}_8$ (Winter et al., 1977). View is along c axis and the black boxes indicate a unit cell.

References

- Ahmadzadeh, M., Marcial, J., and McCloy, J. (2017) Crystallization of iron-containing sodium aluminosilicate glasses in the NaAlSiO_4 - NaFeSiO_4 join. *Journal of Geophysical Research: Solid Earth*, 122, 2504-2524.
- Ballet, O., Coey, J.M.D., Fillion, G., Ghose, A., Hewat, A., and Regnard, J.R. (1989) Magnetic order in acmite; $\text{NaFeSi}_2\text{O}_6$. *Physics and Chemistry of Minerals*, 16, 672-677.
- Baum, E., Treutmann, W., Lottermoser, W., and Amthauer, G. (1997) Magnetic properties of the clinopyroxenes aegirine and hedenbergite: a magnetic susceptibility study on single crystals. *Physics and Chemistry of Minerals*, 24, 294-300.
- Bearden, J.A., and Burr, A.F. (1967) Reevaluation of X-Ray Atomic Energy Levels. *Reviews of Modern Physics*, 39, 125-142.
- Bowen, N.L., and Schairer, J.F. (1938) Crystallization Equilibrium in Nepheline-Albite-Silica Mixtures with Fayalite. *The Journal of Geology*, 46, 397-411.
- Bowen, N.L., Schairer, J.F., and Willems, H.W.V. (1930) The ternary system; Na_2SiO_3 - Fe_2O_3 - SiO_2 . *American Journal of Science, Series 5 Vol. 20*, 405-455.
- Buerger, M.J., Klein, G.E., and Hamburger, G. (1946) Structure of nepheline. *Geological Society of America Bulletin*, 57, 1182-1183.
- Deshkar, A., Marcial, J., Southern, S.A., Kobera, L., Bryce, D.L., McCloy, J.S., and Goel, A. (2017) Understanding the structural origin of crystalline phase transformations in nepheline (NaAlSiO_4) based glass-ceramic. *Journal of the American Ceramic Society*, 100, 2859-2878.

- Di Genova, D., Hess, K.U., Oryaëlle Chevrel, M., and Dingwell, D.B. (2016) Models for the estimation of $\text{Fe}^{3+}/\text{Fe}_{\text{tot}}$ ratio in terrestrial and extraterrestrial alkali-and iron-rich silicate glasses using Raman spectroscopy. *American Mineralogist*, 101, 943-952.
- Di Muro, A., Métrich, N., Mercier, M., Giordano, D., Massare, D., and Montagnac, G. (2009) Micro-Raman determination of iron redox state in dry natural glasses: Application to peralkaline rhyolites and basalts. *Chemical Geology*, 259, 78-88.
- Dunlop, D.J., and Özdemir, Ö. (1977) *Rock magnetism: fundamentals and frontiers*. Cambridge University Press, New York.
- Dunlop, D.J., and Özdemir, Ö. (2007) Magnetizations in rocks and minerals. In M. Kono, Ed. *Geomagnetism, Treatise on Geophysics*, 5, p. 278-331. Elsevier, Amsterdam.
- Edgar, A.D. (1984) Chemistry, Occurrence and Paragenesis of Feldspathoids: A Review. In W.L. Brown, Ed. *Feldspars and Feldspathoids: Structures, Properties and Occurrences*, p. 501-532. Springer Netherlands, Dordrecht.
- Joseph, K., Stennett, M.C., Hyatt, N.C., Asuvathraman, R., Dube, C.L., Gandy, A.S., Govindan Kutty, K.V., Jolley, K., Vasudeva Rao, P.R., and Smith, R. (2017) Iron phosphate glasses: Bulk properties and atomic scale structure. *Journal of Nuclear Materials*, 494, 342-353.
- Lepp, H. (1957) Stages in the Oxidation of Magnetite. *American Mineralogist*, 42, 679-681.
- MacKenzie, W.S. (1957) The crystalline modifications of $\text{NaAlSi}_3\text{O}_8$. *American Journal of Science*, 255, 481-516.
- Martin, R.F. (1969) The hydrothermal synthesis of low albite. *Contributions to Mineralogy and Petrology*, 23, 323-339.
- McMillan, P. (1984) Structural studies of silicate glasses and melts—applications and limitations of Raman spectroscopy. *American Mineralogist*, 69, 622-644.
- Mysen, B.O., and Richet, P. (2005) *Silicate glasses and melts: properties and structure*. Elsevier, Amsterdam.
- Mysen, B.O., and Virgo, D. (1978) Influence of pressure, temperature, and bulk composition on melt structures in the system $\text{NaAlSi}_2\text{O}_6$ - $\text{NaFe}^{3+}\text{Si}_2\text{O}_6$. *American Journal of Science*, 278, 1307-1322.
- Mysen, B.O., Virgo, D., and Scarfe, C.M. (1980) Relations between the anionic structure and viscosity of silicate melts—a Raman spectroscopic study. *American Mineralogist*, 65, 690-710.
- Nestola, F., Tribaudino, M., Boffa Ballaran, T., Liebske, C., and Bruno, M. (2007) The crystal structure of pyroxenes along the jadeite–hedenbergite and jadeite–aegirine joins. *American Mineralogist*, 92, 1492-1501.
- Neuville, D.R., de Ligny, D., and Henderson, G.S. (2014) Advances in Raman spectroscopy applied to earth and material sciences. *Reviews in Mineralogy and Geochemistry*, 78, 509-541.
- Neuville, D.R., and Mysen, B.O. (1996) Role of aluminium in the silicate network: In situ, high-temperature study of glasses and melts on the join SiO_2 - NaAlO_2 . *Geochimica et Cosmochimica Acta*, 60, 1727-1737.
- Phillips, M.W., Ribbe, P.H., and Pinkerton, A.A. (1989) Structure of intermediate albite, $\text{NaAlSi}_3\text{O}_8$. *Acta Crystallographica Section C*, 45, 542-545.
- Prewitt, C.T., and Burnham, C.W. (1966) The crystal structure of jadeite, $\text{NaAlSi}_2\text{O}_6$. *American Mineralogist*, 51, 956-975.
- Ravel, B., and Newville, M. (2005) ATHENA, ARTEMIS, HEPHAESTUS: data analysis for X-ray absorption spectroscopy using IFEFFIT. *Journal of Synchrotron Radiation*, 12, 537-541.
- Rossano, S., and Mysen, B. (2012) Raman spectroscopy of silicate glasses and melts in geological systems. In J. Dubessy, M.-C. Caumon, and F. Rull, Eds. *Raman spectroscopy applied to Earth sciences and cultural heritage*, 12. Mineralogical Society of Great Britain and Ireland.
- Smirnov, A.V., and Tarduno, J.A. (2003) Magnetic hysteresis monitoring of Cretaceous submarine basaltic glass during Thellier paleointensity experiments: evidence for alteration and attendant low field bias. *Earth and Planetary Science Letters*, 206, 571-585.
- Tuttle, O.F., and Bowen, N.L. (1950) High-Temperature Albite and Contiguous Feldspars. *The Journal of Geology*, 58, 572-583.
- Uhlmann, D.R., Yinnon, H., and Cranmer, D. (1980) Crystallization Behavior of Albite. *Lunar and Planetary Science Conference*, p. 1178-1180.
- Wilke, M., Farges, F.o., Petit, P.-E., Brown, G.E., Jr., and Martin, F.o. (2001) Oxidation state and coordination of Fe in minerals: An Fe K-XANES spectroscopic study. *American Mineralogist*, 86, 714-730.
- Winter, J.K., Ghose, S., and Okamura, F.P. (1977) A high-temperature study of the thermal expansion and the anisotropy of the sodium atom in low albite. *American Mineralogist*, 62, 921-931.
- Zanotto, E.D., and Cassar, D.R. (2017) The microscopic origin of the extreme glass-forming ability of Albite and B_2O_3 . *Scientific Reports*, 7, 43022.